Light-Induced Changes in the Structure and Accessibility of the Cytoplasmic Loops of Rhodopsin in the Activated M_{II} State†

Thorsten Mielke,‡ Ulrike Alexiev, M. Gläsel, H. Otto, and M. P. Heyn*

Biophysics Group, Department of Physics, Freie Universität Berlin, Arnimallee 14, D-14195 Berlin, Germany

Received September 28, 2001; Revised Manuscript Received February 18, 2002

ABSTRACT: Bovine rhodopsin was specifically labeled on the cytoplasmic surface at cysteine 140 (the first residue of the loop connecting helices III and IV) or at cysteine 316 (in the loop connecting helix VII and the palmitoylation sites) with the fluorescent labels fluorescein and Texas Red. These loops are involved in activation and signal transduction. The time-resolved fluorescence depolarization was measured in the dark state and in the M_{II} state, with labeled samples consisting of rhodopsin−octylglucoside micelles or rod outer segment (ROS) membranes. In this way the diffusional dynamics of the flexible loops of rhodopsin were measured for the first time directly on the nanosecond time scale. Control experiments showed that the large number of weak excitation pulses required in these single photon counting experiments leads to <5% bleaching of the sample. Rhodopsin was trapped in the activated M_{II} state for the duration of the fluorescence experiments (∼20 min) after illumination at pH 6 and 5 °C. For both types of samples and at both labeled positions the dynamics of the label and loop motion as monitored by the time constants of the depolarization were not significantly different in the two states of the receptor. The end-anisotropy increased, however, from 0.09 in the dark to 0.16 in the M_{II} state for ROS samples labeled at C140. The corresponding numbers for the C316 position are 0.06 and 0.12. Light-induced activation in M_{II} is thus associated with a large increase in the loop steric hindrance due to a changed loop domain structure on the cytoplasmic surface. These results are supported by fluorescence quenching experiments with I^-, which indicate a significant decrease in the collisional quenching constant k_q and in accessibility in the M_{II} state at both positions. The rotational correlation time of the rhodopsin micelles increased from 48 ns in the dark state to 60 ns in M_{II}. This increase is caused by a change in volume and/or shape and is consistent with a structural change. These results demonstrate that time-resolved fluorescence depolarization is a powerful tool to study the changes in conformation and dynamics of the cytoplasmic loops that accompany the activation of rhodopsin and other G-protein coupled receptors.

Rhodopsin is the dim-light photoreceptor of vertebrates (*1*, *2*). It is the prototype of the superfamily of G-protein coupled receptors (GPCR).[1] Understanding the mechanism of activation and signal transduction of rhodopsin is thus of general interest for this class of receptor proteins. Rhodopsin is the only GPCR for which detailed structural information is available. Cryoelectron microscopy has provided two- and three-dimensional structural information at an in-plane resolution of 5 Å (*3*). In these structures the loops that connect the transmembrane helices, and which play an essential role in the mechanism of activation, could not be resolved. Evidence for a loop tertiary structure was obtained from the interaction between spin labels attached to different loops and from disulfide cross-linking experiments (*4*). Recently a high-resolution X-ray diffraction structure was obtained at 2.8 Å resolution (*5*). The N-terminal tail and the loops connecting the transmembrane helices on the extracellular side were fully resolved and shown to adopt a highly ordered tertiary structure (*5*). High crystallographic temperature factors observed for the cytoplasmic loop domain and the lack of several amino acids from the C3 loop and the C-terminal tail, respectively, indicate that this part of the receptor is less structured. Activation, G-protein binding, and signal transduction occur on the cytoplasmic surface. There are three loops on the cytoplasmic side of the membrane, C1, C2, and C3, connecting the following transmembrane helices: I and II (C1), III and IV (C2), and V and VI (C3), respectively. A fourth loop, C4, connects helix VII with the palmitoylation sites at C322 and C323. This loop forms a short amphiphilic helix, called helix VIII, from K311 to L321 that is parallel to the membrane surface (*5*). There is strong evidence that loops C2, C3, and C4 are involved in activation and G-protein binding (*6*−*10*). Light activation is believed to cause a conformational change of the cytoplasmic loop structure allowing transient recognition and binding of signal proteins. Light-induced changes in proximity between pairs of positions in the cytoplasmic domain have been monitored using spin labels. It was shown, for example, that in the

† This work was supported by Grant Sfb 449-TP A5 from the Deutsche Forschungsgemeinschaft (to U.A. and M.P.H.).

* Corresponding author (telephone 49-30-83856141; fax 49-30-83856299; e-mail heyn@physik.fu-berlin.de).

‡ Present address: Medical Research Council, Hills Road, Cambridge CB2 2QH, U.K.

[1] Abbreviations: ROS, rod outer segments; OG, octylglucoside; DTP, 4,4′-dithiodipyridine; GPCR, G-protein coupled receptor; M_I, M_{II}, metarhodopsin I and II; IAF, 5-iodoacetamidofluorescein; TR, Texas Red; EPR, electron paramagnetic resonance; DM, dodecyl maltoside; LM, lauryl maltoside.

10.1021/bi011862v CCC: $22.00
Published on Web 05/29/2002

metarhodopsin II (M_{II}) state the distance between spin labels at the ends of helices III and IV increases by ~5 Å (*11*) and that cross-linking these helices in the dark, by introducing either a disulfide bridge or metal ion binding sites, blocks activation of transducin (*11*, *12*). Light-induced changes in the steady-state electron paramagnetic resonance (EPR) spectra of single spin labels have also been observed at a number of positions, including C140 and C316 in the C2 and C4 loops, respectively (*13*, *14*). EPR studies with rod outer segment (ROS) membranes on the millisecond time scale showed that these spectral changes were associated with the formation and decay of the M_{II} signaling state (*13*). Such methods are not able to detect the rotational diffusion of the loops directly, which occur on a much faster time scale. In this study we report the first observation of the dynamics of the rhodopsin loops in real time on the nanosecond time scale.

Both the structure and dynamics of the cytoplasmic loops of rhodopsin are expected to change upon photoactivation. Despite the well-defined tertiary structure observed for the three-dimensional structure at 100 K (*5*), the loops will have some flexibility and domain motion under physiological conditions at room temperature. These reorientational motions are expected to be anisotropic and sterically constrained by the mutual interactions between the loops as well as between loops and membrane surface. Time-resolved fluorescence depolarization is an appropriate method to monitor such anisotropic and sterically restricted motions. It is a well-established and very sensitive method (*15*, *16*). The principles of this method are simple and theoretically well understood and tested. A short (picosecond) linearly polarized excitation pulse creates a highly anisotropic orientational distribution of excited transition dipole moments (photoselection). The fluorescence emission is accordingly initially highly polarized. This nonequilibrium orientational distribution decays to equilibrium by rotational diffusion. Due to this rotational motion on the time scale of the lifetime of the excited state (typically 10 ns) the high initial fluorescence polarization decays with correlation times that directly reflect the rotational diffusion constants. If the equilibrium orientational distribution is isotropic, the polarization decays to zero. If the equilibrium distribution has some residual order due to sterically restricted motion, the polarization does not decay to zero. The end value of the fluorescence anisotropy r_∞ (a more appropriate measure of the fluorescence polarization) for long times is a measure of the order parameter of the equilibrium orientational distribution (*17*, *18*). The time-resolved fluorescence depolarization signal thus contains dynamic information on the rates at which equilibrium is approached as well as structural information on the degree of steric hindrance. The time resolution allows one to separate these steric and dynamical effects. This is a major advantage over steady-state EPR methods in which only the net effect of these two effects can be observed. These EPR methods are thus similar to steady-state fluorescence depolarization measurements in which the structural and dynamical effects cannot be separated either. Although in principle possible, no time-resolved EPR measurements on the loop dynamics of rhodopsin on the nanosecond time scale have been reported to date.

In the present work we use the two accessible and reactive sulfhydryl groups of the native cysteines C140 (first residue of C2 loop) and C316 (middle of fourth loop, helix VIII) to attach specifically the fluorophores fluorescein and Texas Red. Measurements of the time-resolved fluorescence depolarization then provide information on loop dynamics and structure. These measurements were carried out both in the dark state and in the signaling state M_{II} and showed significant differences. A large decrease in motional freedom was observed in M_{II}. Fluorescence is a versatile method and can also be used to gain complementary information on local polarity and accessibility. Using the wavelength of the emission maximum as a polarity probe, it could be shown that the labels are in a polar environment, as would be expected when they are attached to the cytoplasmic surface. In agreement with this surface location we found that both labels were accessible from the aqueous medium, because the fluorescence could be efficiently quenched by the charged collisional quencher I^-. Interestingly, the labels were significantly less accessible after light activation in the M_{II} state. This is in accordance with the fluorescence depolarization results, which indicate increased steric hindrance in M_{II}.

EXPERIMENTAL PROCEDURES

Materials. Bovine retinae were isolated from fresh cow eyes or were purchased from J. A. Lawson Corp (Lincoln, NE). ConA−Sepharose and Sephadex G25f were from Pharmacia. *N*-Octyl-β-D-glucopyranoside (OG) was from Bachem. Thermolysin and 4,4′-dithiodipyridine (DTP) were purchased from Sigma. 5-Iodoacetamidofluorescein and C_5-bromoacetamido Texas Red were from Molecular Probes.

Methods. (1) Isolation of Bovine ROS and Purification of Rhodopsin. ROS membranes were prepared from fresh bovine retinae at low ionic strength as described (*19*) and purified by discontinuous density gradient centrifugation. To remove other peripheral proteins of the visual cascade, the ROS membranes were washed with NH_4Cl and urea as described (*20*). ROS membranes were solubilized in OG, and the rhodopsin micelles were purified by concanavalin A column chromatography (*21*). Values of the final absorption ratio A_{280}/A_{500} were 1.9−2.0 and 1.7−1.8 for purified ROS membranes and rhodopsin−OG micelles, respectively.

(2) Site Specific Labeling of C140 and C316 with Fluorescein and Texas Red. The fluorescent labels were first dissolved in dimethylformamide (IAF) or dimethyl sulfoxide (TR). Stock solutions of 25 mM concentration were prepared in 10 mM Tris-HCl, pH 7.5. Labeling was performed at a rhodopsin concentration of 25 μM in 10 mM Tris-HCl, pH 7.5, 150 mM NaCl, and, in the case of OG micelles, in the presence of 30 mM OG. The reaction was started by the addition of the label. The molar ratio between label and rhodopsin, the reaction time, and temperature were varied. The reaction was terminated by the addition of 50−100 mM cysteine or gluthatione.

In ROS preparations excess label was removed by repeated washing in 10 mM MES, pH 6.0, 150 mM NaCl until no free label could be detected anymore in the supernatant. In preparations of OG micelles excess label was removed chromatographically using a Sephadex G25f column equilibrated with 10 mM MES, pH 6.0, 150 mM NaCl, and 30 mM OG. Removal of unbound TR required, because of the hydrophobic character of this label, purification over a ConA−Sepharose column. The column was washed with 10

mM MES, pH 6.0, 150 mM NaCl, and 30 mM OG until no free TR was detectable in the effluent. After solubilization, label that was bound to the lipid phase is associated with the dye front on the gels and can be easily detected there by its fluorescence. In this way progress in removal of these label molecules was monitored. Fluorescein could be removed entirely. Small traces of TR remained.

The binding stoichiometry was determined from the absorption difference between labeled and unlabeled rhodopsin at the wavelength of the label absorption maximum. The covalent binding of the fluorescent labels to rhodopsin was established by gel electrophoresis.

Because of its higher reactivity, cysteine 316 was labeled specifically under conditions of low temperature, low molar label/rhodopsin, and short reaction time.

Site-specific labeling of C140 was achieved by blocking C316 with DTP as described (*22*, *23*). ROS membranes were washed and taken up in 10 mM HEPES, pH 6.9, at a rhodopsin concentration of 15−20 μM. Stock solutions of DTP of 50 mM concentration were produced in 10 mM HEPES, pH 6.9. Both solutions were cooled on ice. The reaction was started by the addition of 1 mM DTP. Reaction of the sulfhydryl group of cysteine leads to the formation of 4-thiopyridone. The absorption maximum of DTP is at 247 nm, and that of 4-thiopyridone is at 324 nm (*24*). The course of the reaction can thus be monitored spectroscopically by measuring the absorbance at 324 nm due to 4-thiopyridone using a reference cuvette with 1 mM DTP in 10 mM HEPES, pH 6.9. The extinction coefficient of 4-thiopyridone at 324 nm is 19000 M^{-1} cm^{-1} (*25*). During the course of the reaction the temperature of the sample should not exceed 5 °C to prevent reaction with C140 (see Results). After the reaction of 1−1.1 cysteines per rhodopsin, the reaction was stopped by the addition of 10 mM cysteine and the ROS membranes were washed in 10 mM HEPES, pH 6.9.

Rhodopsin in OG micelles was purified before reaction with DTP by gel filtration over a Sephadex G25f column in 10 mM HEPES, pH 6.9, 30 mM OG. The purpose of this was to remove salts and traces of α-D-methylmannose. C316 was blocked with DTP as described for ROS membranes at a molar excess of 4:1 DTP/rhodopsin in 10 mM HEPES, pH 6.9, 30 mM OG. Excess DTP and 4-thiopyridone were removed chromatographically using a Sephadex G25f column.

(3) Digestion with Thermolysin. Labeled rhodopsin was digested with thermolysin as described (*26*). ROS membranes were first extensively washed to remove salts and then incubated with thermolysin in 10 mM Tris-HCl, pH 7.4, for 4 h at 37 °C in the presence of 5 mM $CaCl_2$. The rhodopsin/thermolysin ratio was 25:1 (w/w). The reaction was stopped by adding EDTA to a final concentration of 20 mM. Rhodopsin in OG micelles was incubated in the same way except that the salt was not removed. The peptide fragments were separated by sodium dodecyl sulfate−polyacrylamide gel electrophoresis according to the method given in ref *27*. After the electrophoresis, the labeled fragments were visualized by their fluorescence, which was documented on a UV fluorescent screen (Polaroid film 667, UV filter 15 orange). Afterward, the bands were stained by Coomassie G250.

(4) Reduction of the Schiff Base by Sodium Borohydride. The Schiff base of rhodopsin was reduced by $NaBH_4$ as described (*28*). An ROS or OG micelle sample (150 μg of rhodopsin in 150 μL) was brought to pH 8.5−9.0 with sodium hydrogen carbonate. At 0 °C, 2.8 mg of $NaBH_4$ was added. Illumination with yellow light (Schott KL1500 lamp with cutoff filter OG 515) led to the formation of the *N*-retinylidene opsin with absorption maximum at 333 nm. The absorption spectrum showed that the reaction was complete after 10 min. Excess reagent was removed by centrifugation (ROS membranes) or gel filtration over Sephadex G25f (OG micelles).

(5) Time-Resolved Fluorescence Depolarization Measurements. These experiments were performed at the synchrotrons BESSY and HASYLAB. The time-resolved fluorescence anisotropy was measured with a home-built setup for time-correlated single photon counting (*29*) designed for use with synchrotron radiation sources. This special design is required due to the change in the impulse response function $L(t)$ of the synchrotron pulses with time. Electron−electron interactions within a bunch and collisions with residual ions lead to a change in pulse shape, intensity, and time position during the several hours of beam storage in the synchrotron. To avoid artifacts due to these changes, the measurements were performed in short cycles. In each cycle the intensities $I_{\parallel}$ and $I_{\perp}$, with analyzers parallel and perpendicular, respectively, to the excitation polarization, were measured for 1 min, followed by a measurement of $L(t)$ for half a minute. Within such a short measuring cycle of several minutes the slowly varying changes of $L(t)$ are negligible. For each cycle $I_{\parallel}$ and $I_{\perp}$ were deconvoluted with $L(t)$ for that cycle. By adding the results from a large number of cycles a sufficient signal-to-noise ratio was achieved. The excitation wavelength was selected from the broad emission spectra of the synchrotron storage rings BESSY I and HASYLAB with a Jobin Yvon monochromator (typical spectral bandwidth = 10 nm). Measurements were performed in the single-bunch modes of the storage rings at 5 MHz, corresponding to a time interval of 200 ns between subsequent excitation pulses. The half-widths of the impulse−response function $L(t)$ were between 600 and 900 ps in BESSY I and ∼200 ps for HASYLAB. A single measuring cycle consisted of consecutive measurement of $I_{\parallel}$, $I_{\perp}$, and $L(t)$. Parallel and perpendicular refer to the orientation of the analyzer with respect to the polarizer. To correct for polarization-dependent differences in sensitivity of the apparatus, the so-called G factor is required in the calculation of the anisotropy $r(t)$. G is determined with the polarizer parallel to the mounting plate (*13*). The G factor was determined before and after the set of cycles and found to lie between 1.000 and 1.050 (±0.003). Usually a time window of 20 ns was selected with a time resolution of 20−25 ps per channel. As a benchmark test for the performance of this setup for anisotropy measurements, the anisotropy of diphenylhexatriene (DPH) in glycerol was measured at −5 °C. An initial anisotropy of 0.39 was obtained.

(6) Analysis of Fluorescence Anisotropy Data. Data analysis was performed as described (*15*). For micelle samples the anisotropy data were fitted to the model function

$$r(t) = \sum_{i=1}^{3} \beta_i \, e^{-t/\phi_i} \qquad (1)$$

For ROS membranes, which do not rotate on the time scale of the fluorescence lifetime, the anisotropy data were fitted

to the model function

$$r(t) = \sum_{i=1}^{2} \beta_i \, e^{-t/\phi_i} + r_\infty \qquad (2)$$

The rotational correlation times ϕ_i provide dynamical information on the rotational motion of the label and the loop to which it is attached. The limiting anisotropy r_∞ is a measure of the degree of rotational constraint and can be used to calculate an order parameter S or cone angle θ as described (*15*, *17*, *30*):

$$r_\infty/r_0 = S^2 = [{}^1/_2 \cos\theta\,(1 + \cos\theta)]^2 \qquad (3)$$

r_0 is the initial anisotropy $r(0)$.

(7) Fluorescence Quenching Measurements. Steady-state fluorescence quenching experiments were carried out using a Kratos RRS 1000 spectrofluorometer. The concentration of the quencher KI was varied from 0 to 70 mM. The monovalent salt concentration was kept constant at 150 mM by adding a corresponding amount of KCl. To prevent the formation of I_3^-, $Na_2S_2O_3$ was added at a concentration of 0.1 mM. The measurements were performed at pH 6 and 10 °C. Because the fluorescence measurements lead to progressive bleaching of the sample, a fresh rhodopsin sample was used at each I^- concentration. To minimize exposure to the excitation light, complete emission spectra were measured at the maximal scan speed of 200 nm/min. An appropriate slit width was chosen to ensure an adequate signal-to-noise ratio. For the calculation of the emitted intensity I, the spectra were numerically integrated. After the dark measurement (<1 min), the sample was bleached for 1 min on ice before the measurement in the M_{II} state. The collisional quenching constant k_q was obtained from a fit of the data to the Stern−Volmer equation:

$$I_0/I = 1 + k_q\bar{\tau}[Q] \qquad (4)$$

In eq 4, [Q] is the quencher concentration, I_0 the emission intensity at [Q] = 0, and $\bar{\tau}$ the mean fluorescence lifetime.

RESULTS

Selective Labeling of C140 or C316 with Fluorescein and Texas Red. By a proper choice of the reaction conditions, in particular of the temperature, pH, ionic strength, and reaction time, either cysteine C140 or C316 could be labeled selectively. The temperature strongly affects the relative reactivity of C140 and C316. This is illustrated in Figure 1, which shows the time course of the reaction of rhodopsin with DTP. The formation of free 4-thiopyridone is monitored by the absorbance at 324 nm. On ice only one cysteine reacts and the reaction goes to completion in ~2 h. Using the absorbance change of 270 mOD at 324 nm, the labeling stoichiometry at this point is about 1:1. Figure 1 shows that increasing the temperature to 25 °C allows the labeling of a second cysteine. The final absorbance change (540 mOD) corresponds to a stoichiometry of approximately 2:1. A very similar time course was observed in ref *23*.

To label either of the two sites specifically with fluorescein or TR, the following procedure was used. The most reactive cysteine (C316, see below) is labeled under conditions of low temperature (on ice), low molar ratio label/rhodopsin, and short reaction time. This led to samples with low labeling

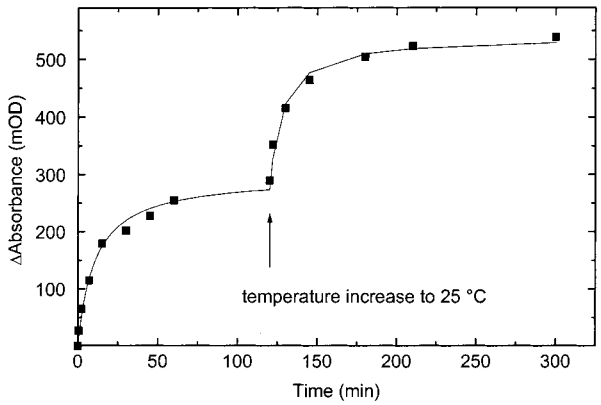

FIGURE 1: Time course of the reaction of rhodopsin with DTP in OG micelles. The reaction was monitored by the absorbance change at 324 nm due to the formation of 4-thiopyridone. The reaction was started on ice by adding a 4-fold excess of DTP. After labeling of one cysteine (C316) per rhodopsin, the temperature was increased to 25 °C. At this higher temperature a second cysteine (C140) can be labeled. Conditions: 20 μM rhodopsin in 10 mM Tris-HCl, pH 6.8, 80 μM DTP.

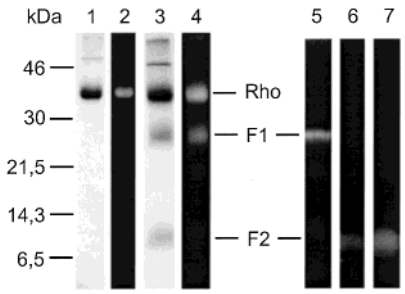

FIGURE 2: Gels of rhodopsin specifically labeled with fluorescein at C140 or C316 before and after proteolytic digestion by thermolysin: (lanes 1 and 2) ROS-C140-AF sample before digestion (lane 1, Coomassie staining; lane 2, fluorescence); (lanes 3 and 4) ROS-C140-AF sample after partial digestion (lane 3, Coomassie staining; lane 4, fluorescence; "Rho", "F_1", and "F_2" mark the positions of the undigested rhodopsin monomer, the F_1 fragment, and the F_2 fragment in the gel, respectively); (lane 5) fluorescence of an OG-C140-AF sample after complete digestion; (lane 6) fluorescence of an OG-C316-AF sample after complete digestion; (lane 7) fluorescence of an ROS-C316-AF sample after complete digestion.

stoichiometries between 0.15 and 0.50. The low stoichiometry is an advantage in the fluorescence experiments, because it reduces the probability of homo energy transfer in ROS membranes (*29*). To label the second cysteine (C140, see below) selectively, cysteine C316 was first quantitatively blocked by the reaction with DTP at 0 °C as described above and under Materials and Methods. The second less reactive site was then labeled at 25 °C under conditions of high molar excess of label to rhodopsin.

The labeling specificity was established by proteolytic digestion with thermolysin. Thermolysin cleaves rhodopsin in the dark mainly at S240 in two fragments F_1 (26 kDa) and F_2 (12 kDa) (*31*). The larger F_1 fragment contains C140, the smaller F_2 fragment C316. Evidence for selective labeling of C316 or C140 with fluorescein is provided by the gels in Figure 2. Lanes 1−4 are for an ROS sample labeled at C140 with fluorescein. Lanes 1 and 2 are the Coomassie staining and fluorescence, respectively, before thermolysin digestion, indicating labeling of the native rhodopsin (38 kDa). Partial digestion leads to three bands marked by Rho, F_1, and F_2 (lane 3). The degradation products F_1 and F_2 have the

expected molecular weights of 26 and 12 kDa, respectively. Lane 4 shows that of the two fragments only F_1 is fluorescent, thus proving that only C140 was labeled. Lane 5 shows the corresponding fluorescence result for a micelle sample OG-C140-AF that was completely digested and indicates that again only C140 was labeled. The corresponding results for the specific labeling of C316 in micelle (OG-C316-AF) and membrane (ROS-C316-AF) samples that were completely digested with thermolysin are shown in lanes 6 and 7, respectively. In this case only the F_2 fragment was fluorescent, consistent with C316 as the labeling site.

Time-Resolved Fluorescence Depolarization in ROS Membranes and OG Micelles. The time-resolved fluorescence depolarization experiments were carried out at the synchrotrons BESSY I and HASYLAB. These synchrotrons provide short light pulses with widths of 700 and 200 ps for BESSY I and HASYLAB, respectively. One advantage of experiments at synchrotrons is the almost unlimited tunability of the excitation light, allowing experiments with a wide range of dyes. This was of particular value for the current investigation because we wanted to test the effect of the label size on the depolarization. A further advantage of synchrotron radiation is that the light is already completely polarized in the plane of the synchrotron. The high pulse frequency of 5 MHz in the single-bunch mode is another important advantage of synchrotron radiation sources. This allows the rapid acquisition of data of sufficient signal-to-noise ratio. This is of particular advantage in the present case with a short-lived M_{II} intermediate, which may be trapped for only 20 min. A key question for experiments with the light-sensitive photoreceptor rhodopsin is whether the large number of short excitation pulses required in single photon counting depolarization experiments (typically 10^{10} pulses) leads to significant bleaching of the sample. The most probable situation for bleaching occurred in our experiments with the fluorescein label, because its absorption (492 nm) and emission (516 nm) maxima are closest to the absorption maximum of bovine rhodopsin (498 nm), thus leading both to efficient direct excitation of rhodopsin and to indirect excitation through energy transfer from the label. Figure 3 shows absorption spectra of a typical sample of rhodopsin labeled with fluorescein before (thin line) and after (thick line) completion of the fluorescence depolarization measurements. The dotted line labels the difference spectrum and indicates that no significant bleaching occurred. The experiments were performed under conditions of maximal light intensity, just after a fresh electron injection in the storage ring at a ring current of 124 mA. The results of Figure 3 show that negligible bleaching (<5%) occurred during the 40 min of the experiment.

Typical results for rhodopsin labeled with fluorescein at cysteine 140 are presented in Figure 4. The data were collected at 15 °C and pH 6. Panel A shows the decay of the anisotropy for ROS membranes labeled at cysteine 140 with fluorescein (ROS-C140-AF). Several phases can be distinguished in the decay. The anisotropy first decays rapidly from an initial value of ~0.39 with a sub-nanosecond correlation time of 0.19 ns (the fit parameters are collected in Table 1). For IAF we obtained under the same experimental conditions a single-exponential decay with a rotational correlation time of 0.19 ± 0.02 ns (data not shown). This time is thus close to the rotational correlation time of free fluorescein and can be assigned to the fast rotational diffusion of the label itself. This rapid decay is followed by a slower

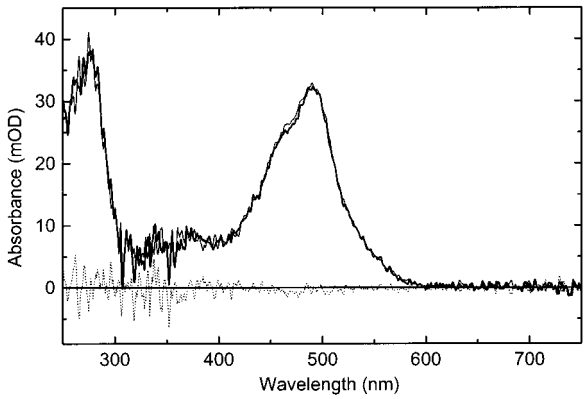

FIGURE 3: Absorption spectra of a fluorescein-labeled rhodopsin sample OG-C316-AF before (thin line) and after (thick line) a complete fluorescence depolarization experiment at the synchrotron HASYLAB. The spectrum is the sum of contributions from rhodopsin and bound fluorescein with maxima at 498 and 492 nm, respectively. The shoulder near 460 nm is due to fluorescein. The amplitude of the difference spectrum (dotted line) at 498 nm is <1 mOD. This shows that the sample was bleached <5% by the excitation pulses during the 40 min of data acquisition at the synchrotron. Conditions: 2 μM rhodopsin in 10 mM MES, pH 6.0, 150 mM NaCl, 30 mM OG, 15 °C.

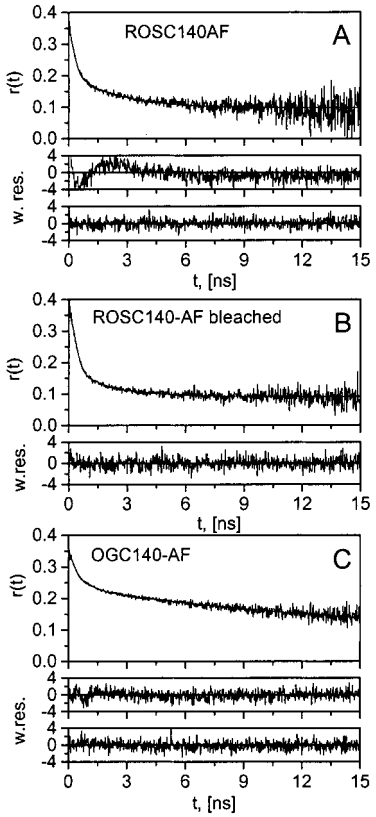

FIGURE 4: Decay of the time-resolved fluorescence anisotropy $r(t)$ of bovine rhodopsin labeled with fluorescein at cysteine 140: (A) ROS membranes; (B) bleached ROS membranes; (C) OG micelles (30 mM OG). Conditions: 10 mM MES, pH 6, 150 mM NaCl, 15 °C. The fitted curves are least-squares fits to eq 2 for (A) and (B) and to eq 1 for (C). The weighted residuals are shown below each panel. For (A) the upper set of residuals is for a fit to one exponential and a constant; the lower set of residuals is for the fit to eq 2. In (B) the residuals refer to the fit to eq 2. In (C) the upper set of residuals is for a fit to two exponentials; the lower set is for the fit to eq 1. The fit parameters are collected in Table 1.

Table 1: Fluorescence Anisotropy Decay Parameters of Fluorescein Bound to Cysteine 140 of Bovine Rhodopsin[a]

	β_1	β_2	β_3	r_∞	ϕ_1 (ns)	ϕ_2 (ns)	ϕ_3 (ns)
ROS-C140-AF	0.18	0.11		0.10	0.19	2.9	
ROS-C140-AF bl	0.22	0.08		0.09	0.17	2.00	
OG-C140-AF	0.07	0.06	0.22		0.10	0.91	30

[a] Conditions: pH 6.0, 150 mM NaCl, 15 °C.

phase with a decay time of 2.9 ns. After ~10 ns, there is no further decay, and the anisotropy remains constant at a value of ~0.1. The fact that the anisotropy does not decay to zero is direct evidence that the rotational motion of the label is sterically hindered on the nanosecond time scale. The fit with eq 2, two exponentials, and a constant end value of r_∞ is adequate, and the residuals are unifomly distributed around zero. These residuals are displayed in the lowest subpanel of Figure 4A. The reduced χ^2_R was 1.13. A fit with only one exponential and a constant leads to a significantly higher χ^2_R value of 2.31 and systematic deviations in the residuals. This is apparent from the middle panel in Figure 4A, which shows the residuals for this model. Systematic deviations occur in the time domain from 0 to 4 ns. For an adequate fit the second exponential is clearly required. In panel B the ROS sample was bleached irreversibly (see Materials and Methods), thereby eliminating the energy transfer between fluorescein and the retinylidene chromophore. As a result the mean fluorescence lifetime $\bar{\tau}$ increased from 1.79 ns in (A) to 3.43 ns in (B). As a consequence there are more counts in the later channels and the signal-to-noise ratio beyond ~7 ns is significantly improved in (B) with respect to that in (A). Comparison between panels A and B shows that bleaching and elimination of the energy transfer have no significant effect on the anisotropy decay. This qualitative observation is supported quantitatively by the comparison of the corresponding fit parameters in Table 1. This is an important control experiment which shows that hetero energy transfer (between label and the retinylidene chromophore of rhodopsin) does not affect the fluorescence depolarization of the label. The advantage of conditions B is that the value of r_∞ can be determined with greater precision. The results for the corresponding OG micelle sample OG-C140-AF are shown in panel C. With micelles there is a third slow decay phase, because the micelles rotate on the fluorescence time scale. The anisotropy therefore does not reach a constant value at the end of the observation window. In this case the fit was made with eq 1, a sum of three exponentials. The necessity of three exponentials is again documented by a substantial drop in χ^2_R in going from a two- (1.21) to a three-exponential (1.02) fit. The residuals in Figure 4C are again only uniformly distributed if we fit to three exponentials. The fit parameters are collected in Table 1. The first time of 0.1 ns is again due to the rapid rotational motion of the label. The last time of 30 ns can be assigned to the rotational diffusion of the OG−rhodopsin micelle. The middle time of 1−2 ns is most likely due to the flexible domain motion at C140.

Light-Induced Changes in Anisotropy at the Cytoplasmic Surface of Rhodopsin at Positions C140 and C316. These experiments were carried out at pH 6, because at this pH the M_I/M_{II} equilibrium is far on the side of M_{II} (e.g. ref *32*). The measurements were performed at 5 °C to prolong the

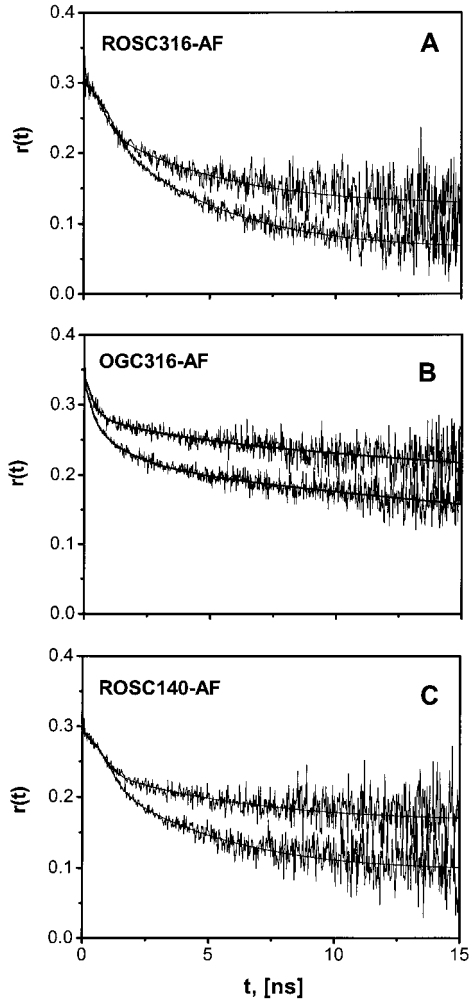

FIGURE 5: Decay of the time-resolved fluorescence anisotropy $r(t)$ of bovine rhodopsin labeled with fluorescein at C140 or C316 in the dark and M_{II} states: (A) ROS-C316-AF; (B) OG-C316-AF; (C) ROS-C140-AF. In each panel the upper trace is for the M_{II} state. Conditions: 10 mM MES, pH 6.0, 150 mM NaCl, 5 °C. The data are fitted to eq 1 for micelle samples or eq 2 for membrane samples. The fit parameters are collected in Table 2.

lifetime of M_{II} sufficiently so that the system remained mostly in M_{II} for the duration of the fluorescence experiments. For the investigation on M_{II} the rhodopsin samples were bleached on ice for 2 min with a cold-light lamp (Schott KL 1500 with cutoff filter OG 515). Immediately afterward the absorption spectra were measured. Using the extinction coefficients of M_I and M_{II} [ϵ_{M_I} (478 nm) = 44000 M^{-1} cm^{-1} and $\epsilon_{M_{II}}$ (380 nm) = 38000 M^{-1} cm^{-1} (*33*)], the equilibrium ratio M_I/M_{II} was calculated to be 0.06 for OG micelles and 0.11 for ROS membranes. The decay of M_{II} at pH 6 and 5 °C was monitored using the absorbance decrease at 380 nm (data not shown). Under these conditions the decay halftime $\tau_{1/2}$ was 90 min for the OG micelle samples and 108 min for ROS membranes. This means that during the period of 15−20 min necessary for the measurement of a fluorescence anisotropy decay curve, only ~8% of the M_{II} population decayed. Figure 5 shows typical data for ROS and micelle samples. The parameters of the fit curves are collected in Table 2. In all three panels the anisotropy decay curve for M_{II} is above that of the dark state. At both positions C140 and C316 the depolarization in M_{II} is significantly reduced compared to the dark state. This is true irrespective of the

Table 2: Fluorescence Anisotropy Decay Parameters of Fluorescein Bound to Cysteine 316 or Cysteine 140 of Bovine Rhodopsin in the Dark State and in the M_{II} Intermediate[a]

	β_1	β_2	β_3	r_∞	ϕ_1 (ns)	ϕ_2 (ns)	ϕ_3 (ns)
ROS-C316-AF							
dark	0.08	0.17		0.06	0.41	4.59	
M_{II}	0.09	0.11		0.12	0.26	4.80	
ROS-C140-AF							
dark	0.08	0.14		0.09	0.44	5.02	
M_{II}	0.07	0.08		0.16	0.37	6.48	
OG-C316-AF							
dark	0.05	0.05	0.24		0.16	1.34	44
M_{II}	0.08		0.26		0.41		50
OG-C140-AF							
dark	0.06		0.24		0.78		64
M_{II}	0.05		0.26		0.74		74

[a] Conditions: pH 6.0, 150 mM NaCl, 5 °C.

type of sample, ROS membrane or OG micelle. For the label at position 316 in ROS membranes (panel A), the data show that the end value of r_∞ is about twice as large in M_{II} as in the dark state, whereas the time constants appear to be unaffected. This is borne out by the fit parameters in Table 2, which show that r_∞ increases from 0.06 in the dark state to 0.12 in M_{II}. The direction of the light-induced effect is the same in ROS membranes at position 140 (panel C). In this case r_∞ increases from a substantially higher value of 0.09 in the dark state to 0.16 in M_{II}. Because the r_0 values are very nearly the same in these four experiments with ROS membranes, we can reach the following conclusions. (1) The degree of orientational constraint in the dark is considerably larger at position C140 than at position C316. This result is not so surprising because C140 is at the membrane interface at the end of helix III and the beginning of the C2 loop, whereas C316 is apparently in a more mobile part of the C4 loop. (2) In the activated M_{II} state the degree of orientational constraint is greatly increased with respect to the dark state, at both positions. Similar results were obtained with OG micelles. Typical results for position C316 are shown in panel B. Again the depolarization is less in M_{II}. The effect is mainly in the amplitude β_3, which increases in M_{II} for both positions (see Table 2). Because the r_0 values are smaller for the C140 than for the C316 measurements, the β_3 values have to be normalized by r_0 to properly compare the orientational constraint at the two positions. In the dark state β_3/r_0 is larger for C140 than for C316, confirming conclusion 1 for micelle samples. The decay time ϕ_3 is due to the rotation of the whole rhodopsin/OG micelle. From Table 2 we conclude that ϕ_3 is larger in M_{II} than in the dark state. This effect was also observed with micelles labeled with TR (data not shown) and, indeed, with any micelle sample investigated. This result shows that the rotational correlation time is larger in M_{II}, suggesting a volume increase or a change in shape.

Light-Induced Changes in Collisional Quenching. The charged collisional quencher I^- was used to investigate the accessibility of the label at position C140 or C316. The experiments were carried out with OG micelles and ROS membranes. Typical results for the sample ROS-C316-AF are shown in Figure 6. Approximately linear Stern−Volmer plots were obtained in all cases over a wide range of quencher concentration. The good linearity of the Stern−Volmer plots both in the dark and in M_{II} (Figure 6) suggests the presence of a single population of fluorophores. As

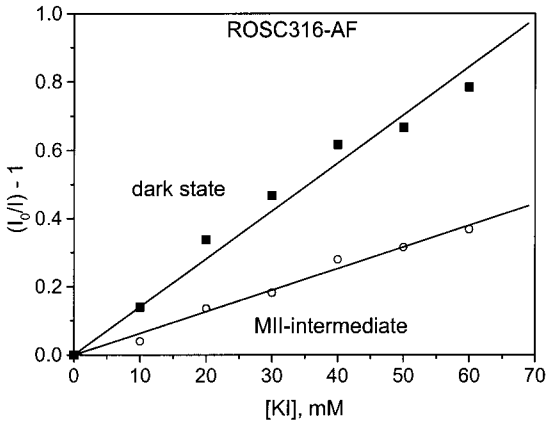

FIGURE 6: Stern−Volmer plot for the sample ROS-C316-AF: (■) dark state; (○) M_{II} state. Conditions: 10 mM MES, pH6, 10 °C. The KI concentration was varied between 0 and 60 mM. The sum of the concentrations of KI and KCl was kept constant at 150 mM.

Table 3: Collisional Quenching Rate k_q of Fluorescein Bound to Position C140 or C316 of Bovine Rhodopsin by I^- (in Units of 10^9 M^{-1} s^{-1})[a]

	OG-C316-AF	OG-C140-AF	ROS-C316-AF	ROS-C140-AF
dark	5.7 ± 0.7	6.2 ± 0.8	5.6 ± 0.7	5.9 ± 0.4
M_{II}	1.5 ± 0.2	2.0 ± 0.2	3.3 ± 0.4	5.4 ± 0.4

[a] Conditions: pH 6.0, 150 mM salt (KCl + KI), 10 °C.

described under Materials and Methods the total salt concentration was kept constant at 150 mM. At a fixed quencher concentration the same sample was used for the measurements in the dark state and in the M_{II} state. Between 9 and 11% of the sample was bleached by the excitation light during the measurements in the dark state. The sample was then put on ice and bleached using a Schott 1500 light source with an OG515 cutoff filter. Because the measurement of one data point takes only 20 s, the sample stayed in the M_{II} state for the duration of the measurement at pH 6 and 10 °C. The slope of the Stern−Volmer plot of Figure 6 is clearly smaller in the activated M_{II} state than in the dark state. For the samples ROS-C140-AF, OG-C316-AF, and OG-C140-AF (data not shown) the results were similar in the sense that the quenching was always less in M_{II}. For dynamic quenching the slope of the Stern−Volmer plot is equal to the product of the collisional quenching constant k_q and the lifetime in the absence of quencher (eq 4). Using the measured mean lifetimes in the dark and M_{II} states, the slopes of the Stern−Volmer plots were converted into quenching constants k_q. The results are presented in Table 3. The numbers in this table are averages of at least two sets of measurements. The errors in k_q take into account the uncertainty in the slope of the linear fit and the error in the lifetime. Except for the sample ROS-C140-AF the results show a significant decrease of k_q in M_{II}. The values in the dark state are within experimental error the same and indicate a high accessibility of the label for the quencher at both positions. The accessibility is clearly smaller in M_{II}. The largest effect occurs at position C316.

DISCUSSION

Our results clearly demonstrate that it is possible to carry out single photon counting fluorescence experiments with light-sensitive photoreceptors such as rhodopsin without

significant bleaching of the sample (Figure 3). Moreover, at a pulse repetition rate of 5 MHz data of sufficient signal-to-noise ratio can be collected in 20 min, thus allowing the study of short-lived trapped photointermediates such as the signaling state M_{II}.

Time-resolved fluorescence depolarization is an appropriate method to monitor the dynamics and steric constraints of the loops of rhodopsin. The anisotropy decay of the bound labels is characterized by a number of decay times. These components reflect a hierarchy of diffusional rotational motions. In the case of ROS membrane fragments the anisotropy decays with two components with rotational correlation times ϕ_1 and ϕ_2 to a nonzero end value of r_∞ (Figure 4A,B). These ROS anisotropy decays are well-described by the model function of eq 2. Two ϕ values are required as judged by the χ^2_R criterium. The fastest time ϕ_1 describes the rotational motion of the small label itself. The intermediate time ϕ_2 of several nanoseconds is due to the motion of the loop and is in good agreement with NMR measurements for flexible domains of other proteins (*29*, *34*). Because ROS membrane fragments do not rotate on the fluorescence time scale, the nonzero value of r_∞ is due to the restricted rotational motion of the labeled loop. The steric hindrance may be due to interactions with adjacent loops or with the membrane surface. In the case of monomeric rhodopsin micelles, $r(t)$ decayed, in addition to the two components with ϕ_1 and ϕ_2, with a third slow component characterized by ϕ_3 (Figure 4C). The micelle anisotropy decays are well-described by the model function of eq 1. Three exponential components are required based on the χ^2_R criterium. The longest time describes the depolarization due to the rotation of the whole micelle.

Using the blocking reaction with DTP, we could selectively label either C140 at the beginning of loop C2 or C316 in the middle of the fourth loop C4. Both of these regions are believed to be involved in molecular recognition and binding of transducin (*6*, *7*, *9*, *10*). The positions of C140 and C316 were recently determined by X-ray diffraction with two-dimensional orthorhombic crystals of rhodopsin that were heavy-atom labeled with *p*-chloromercuribenzoate (*46*). At both positions we found that the loop wobbling motion is sterically constrained, with the effect being more pronounced at C140. Light activation led to a very significant increase in steric hindrance at both positions. This is clear evidence for a change in tertiary structure of the cytoplasmic loop domain with the binding site becoming more constrained. The fact that the three-dimensional rhodopsin crystals decompose upon illumination (*45*) indicates that a structural rearrangement has to take place to form the transducin binding site. This is consistent with our observations of increased steric hindrance in M_{II}. Complementary evidence was obtained from fluorescence quenching experiments with the collisional quencher I^-. At both C140 and C316 the fluorophores become less accessible in the activated M_{II} state. Finally, the rotational correlation time of the micelles was larger in M_{II} than in the dark state, indicating an expansion or a more asymmetric shape after light activation. Because the fluorescence lifetimes of fluorescein and TR are small compared to the micellar tumbling times (~50 ns), the latter have considerable errors. To measure the micellar rotational correlation time more precisely, labels with a longer lifetime are more appropriate. We note that the micellar rotational correlation times in Tables 1 and 2 are in the right ballpark. Using the known volume of rhodopsin and assuming a single shell of OG detergent molecules, we arrive at a rotation time of ~32 ns in water.

Due to the very broad absorption spectrum of rhodopsin, the decay of the anisotropy may be affected by radiationless energy transfer, which occurs on the same time scale. Energy transfer may lead to increased depolarization. Because we are interested in the true anisotropy decay due to loop motions, the possible effects of energy transfer need to be properly understood. In control experiments the effects of energy transfer on the anisotropy decay were thus investigated. By reducing the chromophore with sodium borohydride, we found that hetero energy transfer (between label and retinylidene chromophore) had no significant effect on the fluorescence anisotropy decay (Figure 4A,B). Homo energy transfer, between labels, on the other hand, can lead to substantial depolarization. The effects of homo energy transfer could be entirely prevented in our experiments. No intramolecular homo transfer can occur with rhodopsin micelles that are selectively labeled at either C140 or C316. With ROS membranes intermolecular homo energy transfer could be avoided by working at sufficiently low label stoichiometry.

Recently the structure of the dark state of rhodopsin was solved by X-ray diffraction at a resolution of 2.8 Å (*5*). At the low temperature (100 K) of these experiments the extracellular and cytoplasmic loops have a fairly well-defined tertiary structure (*5*). Ten amino acids in this part of the structure could not be localized at all, and the last 15 amino acids of the carboxyl terminal tail could only be modeled as alanine. The cytoplasmic loops are characterized by high temperature factors (*5*), which are most likely due to the particular crystal packing and the high flexibility of these loops in the inactive state. The diffraction measurements with three-dimensional crystals at 100 K provide a static picture. Our fluorescence depolarization experiments at 15 and 5 °C provide a dynamic picture in real time without the steric constraints due to the crystal contacts. The label rotational motion at C316 is expected to be constrained by the neighboring side chains of N315 and M317 in helix VIII as well as by the membrane surface and the neighboring C-terminal tail. The labeled side chain of C140 may likewise be constrained by the membrane surface, as well as by the side chain of K141 and the neighboring loops. The decrease in motional freedom at both positions upon photoactivation, as deduced from the fluorescence depolarization experiments, suggests that conformational changes occur near C140 and C316. This is in agreement with spin label work and disulfide bond formation, which indicated a light-induced distance increase between the ends of helices III and IV (*11*). Using the same methods, a distance increase was detected upon activation between C316 in helix VIII and H65C in the C1 loop connecting HI and HII (*4*). Further evidence for light-induced structural changes was recently obtained from ^{19}F NMR with rhodopsin labeled with CF_3CH_2S at positions C140 and C316 (*35*). Light-induced changes in the ^{19}F chemical shift were observed with the largest effect occurring at C140 (*35*).

According to the X-ray structure, the fourth loop connecting helix VII and the palmitoylation sites is largely helical. This amphiphilic helix VIII runs from K311 to L321 and is almost parallel to the membrane surface (*5*). C316 is approximately in the middle of this helix with the cysteine side chain about parallel to the membrane (*5*). This could explain the high reactivity of C316 for SH labels and the high accessibility of labeled C316 for the collisional quencher I^-. The increased steric constraint in M_{II} could be caused by a small rotation of helix VIII around its helical axis. The C316 side chain would be turned toward the membrane surface, decreasing the angular freedom and decreasing the accessibility by I^-.

It is of great interest to compare our time-resolved results with those obtained from steady-state EPR experiments with spin labels at positions C140 and C316 (*4*, *13*, *14*, *36*, *37*). In these studies the dynamic state of the side chain was described in a qualitative way by the term "mobility". With this measure of the dynamics the separate effects of the amplitudes and of the rates of motion could not be distinguished in the spectral simulations. Our time-resolved fluorescence depolarization experiments have the advantage that the amplitudes (β_i) and rates of motion (ϕ_i) are directly determined from a fit of the anisotropy according to eq 1 or 2. In contrast to the existing steady-state EPR measurements, time-resolved fluorescence depolarization is able to measure the rotational dynamics directly on the nanosecond time scale. Because extensive data exist with spin labels at both positions and with preparations of ROS membranes and lauryl maltoside (LM) and dodecyl maltoside (DM) micelles, a direct comparison with our data is possible. For the micelle samples preparative differences exist, however. Our experiments were performed with wild-type rhodopsin in OG micelles with the native palmitoylation at C322 and C323 intact. The spin label experiments were performed with DM or LM micelles and initially used samples in which C322 and C323 were not palmitoylated as well as various base mutants. In all spin label studies reported for positions C140 and C316, two populations were observed: an immobilized and a more mobile population. The presence of an immobilized component in the EPR spectra is in good agreement with our results of a positive (nonzero) end anisotropy r_∞ at C140 and C316, indicating considerable steric constraint and limited rotational freedom.

With a spin label at C140 in ROS membranes a clear light-induced increase was observed in the relative amount of the immobilized population (*13*). This is in agreement with our results with both fluorescein and TR (Figure 5), which show a significant light-induced increase in r_∞. In later spin label work with LM and DM micelles, however, the opposite result was obtained: a light-induced increase in mobility at C140 (*14*, *36*, *37*). The reason for this remarkable dependence of the observed light-induced spectral change on the preparation is unclear. One possibility is that the change is lipid dependent and that the difference is due to the unique and unusual lipid composition of the disk membrane. With our fluorescence labels we found, however, both with ROS membranes and with OG micelles an increase in steric constraint at C140 upon photoactivation.

With the spin label at C316 in ROS membranes no significant light-induced change was observed (*13*). With DM micelle samples, on the other hand, an increase in the amount of the immobilized population was observed in M_{II}, regardless of whether there was palmitoylation at C322 and C323 or not (*4*, *14*, *37*, *38*). In our experiments we observed both with OG micelles and with ROS membranes a clear increase in r_∞ in M_{II} corresponding to a more sterically constrained loop motion. This is in agreement with the spin label studies with micelles.

We used the small negatively charged dynamic quencher I^- to probe the accessibility of the fluorescence labels fluorescein and TR bound to the cytoplasmic surface of rhodopsin. As a control we measured the quenching for fluorescein bound to the amino acid cysteine (C-AF) and obtained a collisional quenching constant of 2.4×10^9 M^{-1} s^{-1} (data not shown). This agrees with the value for free fluorescein (*39*). With typical values between 5.6×10^9 and 6.2×10^9 M^{-1} s^{-1} the quenching constant for surface-bound fluorescein in the dark state of rhodopsin is even larger (Table 3). In the activated M_{II} state there is a significant decrease in quenching and accessibility at both positions C140 and C316 (Table 3). The observed difference in slope of the Stern−Volmer plot (Figure 6) cannot be due to the difference in energy transfer, because due to the reduced spectral overlap the mean fluorescence lifetime is larger in M_{II}. These results indicate that some conformational change occurred at these positions. The reduced accessibility in M_{II} may well be associated with the observed reduction in rotational freedom as detected by the increase in r_∞. A small axial rotation of helix VIII, which is approximately parallel to the membrane surface, could, for example, increase the label steric hindrance at C316 and at the same time decrease the accessibility. It is unlikely that the reduced accessibility can be explained as an electrostatic effect, because a proton is taken up in the formation of M_{II}, making the cytoplasmic surface less negatively charged. We note in this connection that a reduced quenching constant with labels on the cytoplasmic surface was also observed in M_{II} with the positively charged quencher *N*-benzylpicolinium (*40*). In these studies the labeling sites were not known. Recently position 250 was labeled with bimane using the mutant V250C (*41*). Using I^- as the quencher, these authors found in M_{II} an increased accessibility at this position near the cytoplasmic end of helix VI. There is no contradiction with our results, as the nature of the structural change in M_{II} is unknown and expected to be different in various regions of the loop domain.

We detected a significant light-induced increase in the slowest rotational correlation time of rhodopsin−OG micelles in M_{II} (ϕ_3 in Table 2). This time is due to the tumbling of the whole detergent−protein complex. The observed effect can be interpreted as a volume increase or as an increase in the asymmetry of the shape. Previous pressure relaxation measurements on the M_I/M_{II} equilibrium have already indicated that the formation of M_{II} is associated with a positive volume change (*42*, *43*) and that this probably involves lateral expansion of rhodopsin in the membrane. Our results are consistent with these studies and indicate that volume changes that are associated with conformational changes may be detected by time-resolved fluorescence depolarization.

Bovine rhodopsin was recently labeled at C316 by Alexa 594, a bulky fluorescent label similar to TR with an absorption maximum of ~588 nm (*44*). Due to its high

extinction coefficient, this label could be excited at 605 nm, that is, to the red of the rhodopsin absorption maximum. This allowed steady-state fluorescence intensity measurements for as long as 30 min with <4% bleaching of rhodopsin. Using their fluorescence assay, these authors showed that the labeled rhodopsin had a normal M_I/M_{II} equilibrium with a pK_a of ~6.8 (*44*). Moreover, in the presence of the fluorescent label at C316, they observed the extra-M_{II} effect upon transducin binding. From competition experiments between labeled and unlabeled rhodopsin for binding of transducin, they concluded that the transducin affinity was comparable. These functional assays thus demonstrate that labeling of C316 by Alexa 594, and presumably also by the smaller fluorescein used in our studies, does not impair the activation of rhodopsin.

CONCLUSIONS AND OUTLOOK

Our experiments have clearly shown the feasibility of doing time-resolved fluorescence depolarization experiments with the light-sensitive photoreceptor rhodopsin both in the dark state and in the signaling state M_{II}. Moreover, with this method the diffusional motion of the flexible loops that are involved in signal transduction is detectable directly on the nanosecond time scale. This allowed for the first time a clear separation of dynamical and steric effects in the mobility. Light-induced increases in the steric constraints of the cytoplasmic loops were detected in the M_{II} intermediate at positions C140 in the C2 loop and C316 in the C4 loop. These changes were accompanied by a reduction in accessibility to quencher. In future studies of this kind with rhodopsin it will be of interest to investigate the effects of phosphorylation, transducin binding, and pH on the loop dynamics. The same method of site-directed fluorescence labeling may also be used to study the loop dynamics of other GPCRs.

ACKNOWLEDGMENT

We thank the management of the synchrotrons BESSY and HASYLAB for providing machine time.

REFERENCES

1. Sakmar, T. P. (1998) *Prog. Nucleic Acid Res. Mol. Biol. 59*, 1−34.
2. Nathans, J. (1992) *Biochemistry 31*, 4923−4931.
3. Krebs, A., Villa, C., Edwards, P. C., and Schertler, G. F. X. (1998) *J. Mol. Biol. 282*, 991−1003.
4. Yang, K., Farrens, D. L., Altenbach, C., Farahbakhsh, Z. T., Hubbell, W. L., and Khorana, H. G. (1996) *Biochemistry 35*, 14040−14046.
5. Palczewski, K., Kumasaka, T., Hori, T., Behnke, C. A., Motoshima, H., Fox, B. A., Le Trong, I., Teller, D. C., Okada, T., Stenkamp, R. E., Yamamoto, M., and Miyano, M. (2000) *Science 289*, 739−745.
6. König, B., Arendt, A., McDowell, J. H., Kahlert, M., Hargrave, P. A., and Hofmann, K. P. (1989) *Proc. Natl. Acad. Sci. U.S.A. 86*, 6878−6882.
7. Franke, R. R., Sakmar, T. P., Graham, R. M., and Khorana, H. G. (1992) *J. Biol. Chem. 267*, 14767−14774.
8. Cai, K., Klein-Seetharaman, J., Farrens, D. L., Zhang, C., Altenbach, C., Hubbell, W. L., and Khorana, H. G. (1999) *Biochemistry 38*, 7925−7930.
9. Ernst, O. P., Meyer, C. K., Marin, E. P., Henklein, P., Fu, W.-Y., Sakmar, T. P., and Hofmann, K. P. (2000) *J. Biol. Chem. 275*, 1937−1943.
10. Marin, E. P., Krishna, A. G., Zvyaga, T. A., Isele, J., Siebert, F., and Sakmar, T. P. (2000) *J. Biol. Chem. 275*, 1930−1936.
11. Farrens, D., Altenbach, C., Yang, K., Hubbell, W., and Khorana, H. G. (1996) *Science 274*, 768−770.
12. Sheikh, S., Zvyaga, T. A., Lichtarge, O., Sakmar, T. P., and Bourne, H. R. (1996) *Nature 383*, 347−350.
13. Farahbakhsh, Z. T., Hideg, K., and Hubbell, W. L. (1993) *Science 262*, 1416−1419.
14. Resek, J. F., Farahbakhsh, Z. T., Hubbell, W. L., and Khorana, H. G. (1993) *Biochemistry 32*, 12025−12032.
15. Heyn, M. P. (1989) *Methods Enzymol. 172*, 462−471.
16. Lakowicz, J. R. (1999) *Principles of Fluorescence Spectroscopy*, Kluwer Academic/Plenum Publishers, New York.
17. Heyn, M. P. (1979) *FEBS Lett. 108*, 359−364.
18. Lipari, G., and Szabo, A. (1980) *Biophys. J. 30*, 489−506.
19. McDowell, J. H., and Kühn, H. (1977) *Biochemistry 16*, 4054−4060.
20. Yamanaka, G., Eckstein, F., and Stryer, L. (1985) *Biochemistry 24*, 8094−8101.
21. De Grip, W. J. (1982) *Methods Enzymol. 81*, 197−207.
22. Chen, Y. S., and Hubbell, W. L. (1978) *Membrane Biochem. 1*, 107−130.
23. Albert, A. D., Watts, A., Spooner, P., Groebner, G., Young, J., and Yeagle, P. L. (1997) *Biochim. Biophys. Acta 1328*, 74−82.
24. Grassetti, D. R., and Murray, J. F. (1967) *Arch. Biochem. Biophys. 119*, 41−49.
25. Cai, K., Langen, R., Hubbell, W. L., and Khorana, H. G. (1997) *Proc. Natl. Acad. Sci. U.S.A. 94*, 14267−14272.
26. Pober, J. S. (1982) *Methods Enzymol. 81*, 236−239.
27. Laemmli, U. K. (1970) *Nature 227*, 680−685.
28. Bownds, D., and Wald, G. (1965) *Nature 205*, 254−257.
29. Kelly, L. A., Trunk, J. G., and Sutherland, J. C. (1997) *Rev. Sci. Instrum. 68*, 2279−2286.
30. Kinosita, K., Kawato, S., and Ikegami, A. (1977) *Biophys. J. 20*, 289−305.
31. Findlay, J. B., Barclay, P. L., Brett, M., Davison, M., Pappin, D. J., and Thompson, P. (1984) *Vision Res. 24*, 1301−1308.
32. Dickopf, S., Mielke, T., and Heyn, M. P. (1998) *Biochemistry 37*, 16888−16897.
33. Kibelbek, J., Mitchell, D. C., Beach, J. M., and Litman, K. J. (1991) *Biochemistry 30*, 6761−6768.
34. Epstein, D. M., Benkovic, S. J., and Wright, P. E. (1995) *Biochemistry 34*, 11037−11048.
35. Klein-Seetharaman, J., Getmanova, E. V., Loewen, M. C., Reeves, P. J., and Khorana, H. G. (1999) *Proc. Natl. Acad. Sci. U.S.A. 96*, 13744−13749.
36. Farahbakhsh, Z. T., Ridge, K. D., Khorana, H. G., and Hubbell, W. L. (1995) *Biochemistry 34*, 8812−8818.
37. Kim, J.-M., Altenbach, C., Thurmond, R. L., Khorana, H. G., and Hubbell, W. L. (1997) *Proc. Natl. Acad. Sci. U.S.A. 94*, 14273−14278.
38. Altenbach, C., Cai, K., Khorana, H. G., and Hubbell, W. L. (1999) *Biochemistry 38*, 7931−7937.
39. Johnson, D. A., and Yguerabide, J. (1985) *Biophys. J. 48*, 949−955.
40. Borochov-Neori, H., and Montal, M. (1983) *Biochemistry 22*, 197−205.
41. Dunham, T. D., and Farrens, D. L. (1999) *J. Biol. Chem. 274*, 1683−1690.
42. Lamola, A. A., Yamane, T., and Zipp, A. (1974) *Biochemistry 13*, 738−745.
43. Attwood, P. V., and Gutfreund, H. (1980) *FEBS Lett. 119*, 323−326.
44. Imamoto, Y., Kataoka, M., Tokunaga, F., and Palczewski, K. (2000) *Biochemistry 39*, 15225−15233.
45. Okada, T., Le Trong, I., Fox, B. A., Behnke, C. A., Stenkamp, R. E., and Palczewski, K. (2000) *J. Struct. Biol. 130*, 73−80.
46. Mielke, T., Villa, C., Edwards, P. C., Schertler, G. F. X., and Heyn, M. P. (2002) *J. Mol. Biol. 316*, 693−709.

BI011862V